Ultrafast carrier relaxation in GaN, $In_{0.05}Ga_{0.95}N$, and an $In_{0.07}Ga_{0.93}N/In_{0.12}Ga_{0.88}N$ multiple quantum well

Ümit Özgür and Henry O. Everitt*
Department of Physics, Duke University, Durham, North Carolina 27708
(Received 16 September 2002; revised 8 January 2003; published 11 April 2003)

Room-temperature, wavelength-nondegenerate ultrafast pump/probe measurements were performed on GaN and InGaN epilayers and an InGaN multiple quantum well (QW) structure. Carrier relaxation dynamics were investigated as a function of excitation wavelength and intensity. Spectrally resolved sub-picosecond relaxation due to carrier redistribution and QW capture was found to depend sensitively on the wavelength of pump excitation. Moreover, for pump intensities above a threshold of 100 $\mu J/cm^2$, all samples demonstrated an additional emission feature arising from stimulated emission (SE). SE is evidenced as accelerated relaxation (<10 ps) in the pump-probe data, fundamentally altering the redistribution of carriers. Once SE and carrier redistribution is completed, a slower relaxation of up to 1 ns for GaN and InGaN epilayers, and 660 ps for the multiple QW sample, indicates carrier recombination through spontaneous emission.

DOI: 10.1103/PhysRevB.67.155308 PACS number(s): 78.47.+p, 78.66.Fd, 78.45.+h, 78.67.De

I. INTRODUCTION

Technological advances in group-III nitride-based optoelectronics have been possible with extensive materials research, resulting in the commercialization of short-wavelength emitters and detectors.[1–4] The active layers in high efficiency emitters, such as blue/green light emitting diodes and blue/purple laser diodes, contain InGaN alloys. Time scales for carrier recombination, transport, and quantum well (QW) capture in the ultrafast regime determine the efficiency of optoelectronic devices. Therefore it is important to understand the carrier relaxation and recombination mechanisms in InGaN structures. In addition to many studies on recombination times,[5–7] there have been a limited number of reports on ultrafast carrier dynamics in InGaN heterostructures[8,9] and multiple quantum wells (MQWs).[10,11] Measurements on heterostructures, single QWs, and MQWs have emphasized different aspects of carrier relaxation in nitrides. In this paper, we report comprehensive room temperature ultrafast measurements on GaN and InGaN epilayers, and an InGaN MQW sample.

In achieving the current state of nitride device development, overcoming material growth difficulties has been the main focus. The efficiencies of InGaN-based emitters are strongly affected by material inhomogeneities such as compositional fluctuations and indium-phase separation. However, inhomogeneities in the form of quantum dot-sized In-rich regions are observed to increase lateral confinement, thereby increasing the emission efficiencies of InGaN devices. The effect of these In-rich regions on electron-hole recombination through spontaneous emission (SPE) has been studied extensively.[5,12,13] In spite of imperfect material properties, high emission efficiencies are observed not only through enhanced SPE but also through stimulated emission (SE) generated at moderate pump powers. There have been many reports on SE in InGaN epilayers[14,15] and MQW structures.[16–18] However SE and its effects on carrier relaxation are poorly understood. In this study, ultrafast dynamics in the presence and absence of SE are investigated.

Three samples, a GaN epilayer, an InGaN epilayer, and an InGaN MQW structure, were grown on *c*-plane double polished sapphire by metal-organic chemical vapor deposition at the University of California, Santa Barbara.[19] The GaN sample was ~ 3 μm thick, and the buffer layers in the other two samples were ~ 2 μm-thick GaN:Si. The InGaN epilayer sample consisted of a 60 nm-thick $In_{0.05}Ga_{0.95}N$:Si layer, capped with another 15 nm-thick GaN layer. The InGaN MQW was a typical laser active layer structure with 10 periods of 8.5 nm $In_{0.07}Ga_{0.93}N$:Si barriers and 3.5 nm $In_{0.12}Ga_{0.88}N$ quantum wells. There was a 100 nm GaN cap layer on top of the MQW. The doping in the barriers and in the InGaN epilayer was $\sim 10^{18}$ cm^{-3}.

In Sec. II, techniques used in the experiment are introduced. Then the results for each sample are respectively considered as subsections of Sec. III. In each subsection, first continuous-wave and time-integrated measurements are presented to identify the band structures. The investigation of carrier relaxation dynamics follows, using nondegenerate time-resolved differential transmission (TRDT) spectroscopy. To understand the effects of the underlying buffer and cap GaN layers, and to understand the effects of the three-dimensional (3D) InGaN barriers in the MQW sample, measurements of the GaN and InGaN epilayer samples are discussed, respectively. Above and below band gap excitation data are presented to explore the excitation wavelength dependence of the GaN and InGaN relaxation phenomena.

Similarly, measurements on the MQW sample are reported for above-, at-, and below-barrier energy excitations. Time-resolved data for the MQW sample are compared with results from a previous study of carrier capture times using degenerate TRDT.[20]

II. EXPERIMENTAL TECHNIQUES

A. Continuous-wave and time-integrated characterization

Continuous-wave (cw) photoluminescence (PL), PL excitation (PLE), and absorption measurements were performed at room temperature. cw PL was measured at excitation

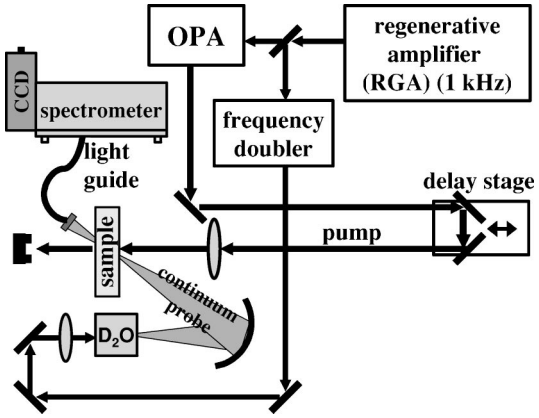

FIG. 1. Experimental setup for nondegenerate TRDT.

power densities of 100 W/cm^2 using a 25 mW HeCd laser operating at 325 nm (3.82 eV). A 300 W Xe lamp was used for PLE and cw-absorption measurements. The Xe lamp was dispersed by a 30 cm double-grating spectrometer for the PLE, and both cw PL and PLE were detected by a photomultiplier tube attached to a 75 cm grating spectrometer. Another 30 cm grating spectrometer with a charge coupled device (CCD) was used for the absorption measurements.

Pulsed excitation, time-integrated PL (TI PL) was performed on the samples at room temperature using 1 kHz, ~ 10 μJ pulses from an optical parametric amplifier, at excitation power densities varied between 20 μJ/cm^2 and 2 mJ/cm^2 either by changing the focus or using neutral density filters. For high enough excitation densities, SE features were observed for all the samples. To obtain the SE threshold densities, PL from the samples was detected both normal to the surface from the front and parallel to the surface from the edges. Edge detection produced stronger SE signals, making it the preferred detection scheme. The samples were excited normal to the surface, and the PL was collected from the edge using a 600 μm diameter ultraviolet-visible fiber. A CCD attached to the 30 cm spectrometer was used for detection. Both the spectrally integrated PL intensity and the emission linewidth were plotted as a function of pump energy density and found to give identical SE thresholds.

B. Time-resolved characterization

Previously, standard wavelength-degenerate TRDT measurements were performed on the MQW sample, using a frequency-doubled mode-locked Ti:sapphire laser.[20] In this study, nondegenerate TRDT spectroscopy was applied at room temperature. The experimental setup is shown in Fig. 1. A Ti:sapphire laser-seeded, 1 kHz Quantronix Titan regenerative amplifier (RGA) with 1.8 mJ, 100 fs pulses at 800 nm was used. Half of the RGA output power was used to pump a Quantronix TOPAS optical parametric amplifier (OPA). The signal output from the tunable OPA was frequency quadrupled and used as the pump in the differential transmission (DT) experiment. The other half of the RGA output was frequency doubled in a Beta Barium Borate (BBO) crystal and focused on a quartz cell filled with D_2O to generate a broadband continuum probe centered near 400 nm (3.11 eV). The continuum probe, which had relatively minor amplitude fluctuations over its >100 nm bandwidth, was highly attenuated by spatial filtering, then collected and focused on the sample using a spherical mirror. The pump beam was delayed with respect to the probe beam using a retroreflector mounted on a 1 μm-resolution translational stage. The probe, transmitted through the sample, was then collected by a UV liquid light guide, sent to the 30 cm grating spectrometer, and detected by a CCD camera attached to the output port. It is important to note that the excitation regime in this study was much higher (>100 μJ/cm^2) than that of the previous study of degenerate TRDT (~ 1 μJ/cm^2).[20] Using a pump intensity-independent absorption constant of 10^5 cm^{-1},[21] the number of photoinjected carriers in the MQW sample was estimated to be 10^{17} cm^{-3} for the previous study and $>10^{19}$ cm^{-3} for this work.

First, the continuum probe spectrum was recorded. Next, the pulsed absorption spectrum of the sample was obtained by comparing the continuum probe spectrum and the spectrum of the probe transmitted through the unpumped sample. Some absorption features that were not clear in the cw-absorption data were easily observed in the pulsed absorption spectra due to larger excitation density. Then, pump-probe measurements were made by comparing the transmission of the probe through the sample with and without the pump beam for various delays up to 0.4 ns. The absolute DT signal at energy $h\nu$ was

$$DT(h\nu)=\frac{T_{PumpON}(h\nu)-T_{PumpOFF}(h\nu)}{T_{PumpOFF}(h\nu)}=-\triangle\alpha(h\nu)d, \tag{1}$$

where T_{PumpON} and $T_{PumpOFF}$ are the probe transmission signal magnitudes with the pump beam turned on and off, respectively. $\triangle\alpha$ is the change in the absorption coefficient, and d is the thickness of the sample over which the change in absorption is induced. Pump and probe spot diameters on the samples were ~ 1 mm and ~ 0.2 mm, respectively. The absorption from the bare probe beam was observed to be much smaller than the absorption due to the pump beam, suggesting that the modulation in the DT signal is purely from the pump.

TRDT data is presented in two different ways, spectrally integrated and spectrally resolved, in order to elucidate different aspects of the relaxation processes. Spectrally integrated DT gives an indication of the total population of carriers and their aggregate decay, while spectrally resolved DT describes the distribution of carriers and indicates their energy relaxation pathways.

Due to the thick GaN layers, strong absorption at the GaN band edge allows only weak transmission of the probe beam for all the samples. Therefore, a small pump-induced change in the absorption at the GaN energy will yield a large TRDT signal. Spectrally resolved TRDT data for all the samples show oscillations that arise from the interference of the multiple reflections in the sample.

Similar nondegenerate TRDT measurements have been performed on GaN,[22,23] InGaN epilayers,[8,9] and InGaN MQWs,[9–11,24] by different groups. These studies provide in-

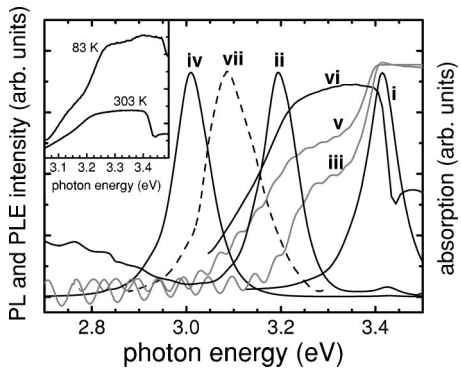

FIG. 2. Room temperature cw PL (i) for the GaN sample, cw PL (ii) and absorption (iii) for the InGaN sample, cw PL (iv), cw absorption (v), PLE (vi), and time-integrated pulsed PL (vii) for the MQW sample. The excitation density for the pulsed PL is above ($\sim$2 mJ/cm^2) the SE threshold. The inset shows the log scale plot of the 83 K and 303 K PLE for the MQW sample.

sight into important aspects of carrier relaxation dynamics. In this study, a more comprehensive, comparative investigation was made for all three types of samples, focusing on relaxation over many time scales, sub-picosecond to nanosecond, as a function of excitation wavelength and density. The role of stimulated emission on carrier dynamics is also studied in both spectrally integrated and spectrally resolved data.

III. RESULTS AND DISCUSSION

A. Differential transmission of a GaN epilayer

As seen in Fig. 2, the cw PL from the GaN sample is centered at 3.41 eV when excited at 3.82 eV, above the band gap, in agreement with the 3.41 eV GaN band edge obtained from pulsed absorption measurements. Pulsed PL showed another peak at 3.31 eV due to electron-hole plasma (EHP) induced SE,[25–27] with a threshold of 70 μJ/cm^2. The 3.31 eV SE peak is observed to redshift by 25 meV and broaden from 37 meV to 66 meV as pump intensity increases from 40 μJ/cm^2 to 2 mJ/cm^2. When the sample is excited at 3.34 eV, below the band gap, no PL is observed.

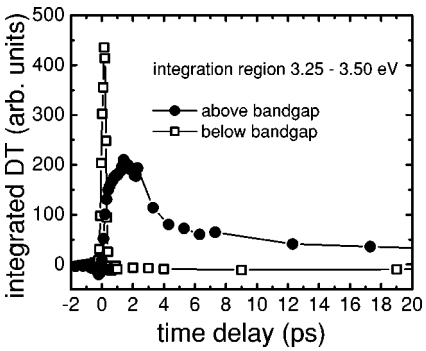

FIG. 3. Time evolution of the spectrally integrated TRDT for above (circles) and below (squares) band gap excitations of the GaN epilayer sample at an excitation energy density of 300 μJ/cm^2. The integration region was 3.25 eV–3.50 eV.

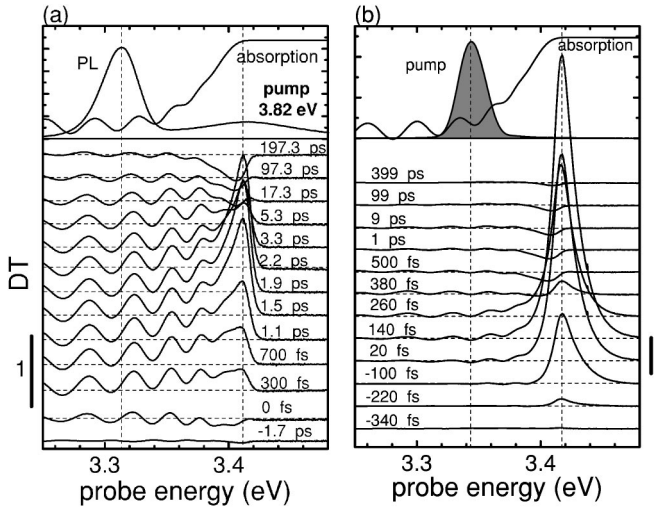

FIG. 4. Spectrally resolved TRDT for above (a) and below (b) band gap excitations of the GaN epilayer sample at various delays for an excitation density of 300 μJ/cm^2. The top graphs show the pump spectrum, the TI PL, and the pulsed absorption. The vertical bars on the sides indicate a DT magnitude of 1.

The spectrally integrated TRDT data for the GaN at excitation energies 410 meV above (3.82 eV) and 70 meV below (3.34 eV) the band gap are shown in Fig. 3. For below band gap excitation, increased transmission is observed for a very short time, less than 1 ps. Data for the above band gap excitation shows a similarly rapid rise, a $\sim$2 ps-wide peak, and a fast, 3–6 ps lasting decay, followed by a much slower relaxation lasting hundreds of ps. For both excitations, the early, strong increase in transmission at the GaN band edge is due to photoexcited carriers and the dynamic (ac) Stark effect.[22,28] The wide peak and fast relaxation are due to the operation and removal of carriers through SE, which occurs when the pump density is above the threshold of 70 μJ/cm^2 and ends when the number of carriers is reduced below threshold. The time constant for SE decay at an excitation density of 300 μJ/cm^2 is measured to be $\sim$2 ps.

Spectrally resolved results from the TRDT measurements on the GaN sample, shown in Fig. 4, confirm these findings for excitations above and below the GaN band edge. For excitation 410 meV above the band gap [Fig. 4(a)], the carrier distribution is broad ($\sim$80 meV) and extends $\sim$100 meV below the band gap during the first 1.2 ps. The carriers relax to the GaN band edge in $\sim$2 ps through multiple LO-phonon and carrier scattering events required to cool the carriers by 410 meV.[29] The 2 ps-wide SE feature in the spectrally integrated DT is observed during this cooling. After 2 ps when the carrier redistribution is finished, a clear decay due to SE becomes visible, with a decay constant of $\sim$2 ps. By 17 ps, the lower-energy part (3.30 eV–3.37 eV) of the distribution disappears, while carriers near the GaN band edge show increasing absorption. The decay of the low-energy part might be explained by the blueshift of the SE from the EHP as the number of carriers decreases through SE. This is supported by the fact that SE has been observed to redshift with increasing carrier density due to increased Coulombic repulsion.[26]

For excitation 70 meV below the band gap, shown in Fig. 4(b), the generation of carriers may seem more surprising, especially because it cannot be explained as an assist from room-temperature thermal energy k_BT (26 meV) or from the pulse bandwidth (25 meV). It is well known that the excitonic resonances are visible even at room temperature for GaN,[21] and the ac Stark effect has been observed for GaN for detunings as large as 159 meV below the excitonic resonance.[28] The bleaching which exists during the intense pump pulse and lasts less than 500 fs is an indication of the ac Stark effect. This short-lived ac Stark feature in Fig. 4(b) is observed in all the samples as a very fast increase and decay of the spectrally integrated DT for below band gap excitations (e.g., see Fig. 3). The residual change in the DT which persists as long as 400 ps is due to real excitation of carriers by the two-photon absorption of the intense pump pulse (300 μJ/cm^2).

At longer delays, induced absorption is observed at the GaN energy for both above and below band gap excitations. The observed slow relaxation is due to decaying remnant carriers and excitons at the GaN band edge. The rate of this decay is observed to be slower than 300 ps, which is consistent with the recombination lifetimes obtained for GaN.[21,27]

B. Differential transmission of an $In_{0.05}Ga_{0.95}N$ epilayer

Figure 2 shows the PL emission from the $In_{0.05}Ga_{0.95}N$ epilayer, which occurred at ~3.20 eV for cw excitation (100 W/cm^2) from the 3.82 eV HeCd laser. This is slightly lower than the band gap values for $In_{0.05}Ga_{0.95}N$ in the literature, constrained between 3.220 eV and 3.224 eV.[30,31] TI PL is only observed for above band gap excitation, never for below band gap excitation. The cw absorption also shown in Fig. 2 suggests an $In_{0.05}Ga_{0.95}N$ band edge of 3.26 eV. When the broadening of the band edge is taken into account, an effective band edge of 3.22 eV is obtained from a sigmoidal fit,[12] giving a 20 meV Stokes shift. Since the piezoelectric (PZE) field in the InGaN epilayer is already reduced with Si doping,[7] the band edge changes very little with pulsed laser excitation. Thus, screening of the PZE field does not produce a remarkable blueshift. This is verified by pulsed absorption measurements which suggest an $In_{0.05}Ga_{0.95}N$ band edge of ~3.26 eV, similar to the cw absorption.

The spectrally resolved TRDT data for the InGaN sample is shown in Fig. 5. Pump wavelengths for Fig. 5(a) and Fig. 5(b) were 90 meV above (3.35 eV) and 30 meV below (3.23 eV) the InGaN band gap, respectively. Before considering carrier dynamics in the InGaN layer, it is useful to reconsider carrier dynamics in the GaN layers in this sample. The pump energies are 60 meV, and 180 meV below the GaN band gap, respectively. As in the below band gap data for the GaN sample [Fig. 4(b)], it is first observed that the transmission increases from carrier generation and ac Stark effect in the GaN, reaching a maximum in ~300 fs at the 3.41 eV GaN band edge for both pump energies. The ac Stark effect is observed in the GaN layers of the InGaN epilayer sample in a manner similar to the below band gap excitation of the GaN sample. The magnitude of the ac Stark effect is smaller for the larger detuning of 180 meV in Fig. 5(b). Real carriers

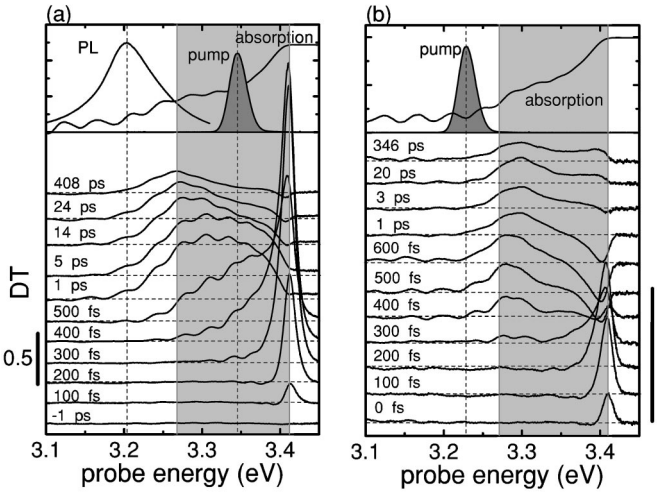

FIG. 5. Spectrally resolved TRDT for above (a) and below (b) band gap excitations of the InGaN epilayer sample at various delays for an excitation density of 300 μJ/cm^2. The top graphs show the pump spectrum, the TI PL, and the pulsed absorption. The shaded regions indicate the states between InGaN and GaN band edges. The vertical bars on the sides indicate a DT magnitude of 0.5.

are also generated at the GaN band edge due to two-photon absorption, but unlike the GaN sample they can quickly (<1 ps) decay into lower InGaN states through carrier-LO-phonon and carrier-carrier scattering processes. This makes the distinction between the two-photon absorption and the ac Stark effect more difficult. The small decreases (above band gap) or increases (below band gap) in absorption at the 3.41-eV GaN band edge after 5 ps are due to the remnant carriers and excitons at the GaN interface and trap states. The two-photon-induced carrier absorption feature in the GaN sample [Fig. 4(b)] remains visible after 408 ps with little reduction in amplitude. This contrasts with the more complex relaxation observed in the GaN cap and buffer layers of the InGaN sample [Fig. 5(b)] which varies between induced absorption and transmission with excitation energy and time but remains for at least 400 ps. The differences can be attributed to carrier relaxation from the GaN layers to the InGaN epilayer and the reduced role of SPE in the GaN layers and trap states.

Regarding carrier dynamics in the InGaN layer, SE appears at 3.21 eV, near the InGaN band edge and 10 meV on the blue side of the PL, for excitation 90 meV above the InGaN band gap. Since the SE peak is broad and very close to the main PL peak, the onset of SE is observed as the emergence of a narrower-linewidth PL feature whose strength increases with increasing pump intensity. From PL measurements of spectrally integrated intensity and linewidth, a pump threshold of ~80 μJ/cm^2 is obtained. Spectrally integrated TRDT data for above band gap, above threshold (300 μJ/cm^2) excitation in Fig. 6 shows a fast decay during the first 14 ps due to carrier removal through SE, followed by a much slower relaxation through SPE after the carrier density decreases below the SE threshold. The fast rising edge of the spectrally integrated DT for both excitations includes the contribution from the ac Stark effect at the GaN band edge, as observed in Fig. 3.

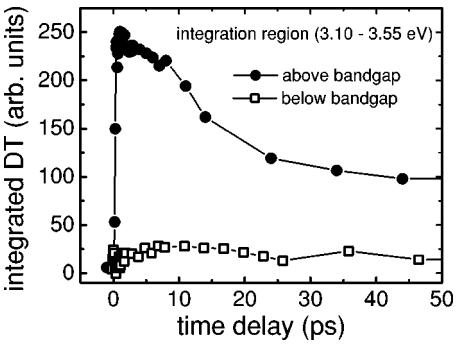

FIG. 6. Time evolution of the spectrally integrated TRDT for above (circles) and below (squares) band gap excitations of the InGaN epilayer sample at an excitation density of 300 μJ/cm^2. The integration region was 3.10 eV–3.55 eV.

The fast relaxation feature of the spectrally integrated TRDT is spectrally resolved in Fig. 5(a) as a redistribution of the carriers. The broad distribution of carriers becomes clearly visible after 400 fs as a bleaching of the InGaN photoabsorption. The carrier distribution extends from the GaN band edge to the InGaN band edge and reaches a maximum in 1 ps at $\sim$3.30 eV. Afterwards, the blue edge of this bleaching, $\sim$70 meV above the InGaN band edge, is observed to decay rapidly ($<$14 ps) while the red edge (3.18–3.27 eV) remains almost constant. The redshift of the bleaching arises from carrier cooling, and the peak reaches the 3.26-eV $In_{0.05}Ga_{0.95}N$ band edge by 14 ps when SE ceases. Thus the fast decay feature of the spectrally integrated TRDT is due to the fast removal of the carriers at the InGaN band edge through SE, while carriers at higher energies relax down to refill the lost carriers. After the number of carriers is reduced below the SE threshold, only SPE remains.

By contrast, for excitation 30 meV below the InGaN band gap, SE is not observed, and the DT signal, shown in Fig. 5(b), does not exhibit SE-related features. The number of induced carriers is smaller, and the DT signal shows them narrowly distributed close to the band edge, reaching a maximum in 600 fs. Of particular noteworthiness is the absence of the SE-mediated fast decaying blue edge seen in above band gap excitation. During the first 3 ps, there is also a more complex absorption change at the GaN band edge due to a combined effect of the ac Stark effect and the two-photon absorption. Induced absorption is observed between 0.4 and 3 ps, and increased transmission at the GaN energy persists for as long as 346 ps due to carriers and excitons in GaN trap states.

Spectrally integrated DT data for both excitation energies show an additional decay component in the InGaN with a much larger time constant of several 100 ps. Spectrally resolved TRDT reveals that carriers decay very slowly, and the carrier distribution continues to narrow, after 24 ps in above band gap excitation [Fig. 5(a)] and after 600 fs in below band gap excitation [Fig. 5(b)]. The slow decay of these cooled carriers is due to radiative recombination-induced SPE. From the data, the radiative recombination time in this InGaN layer is estimated to be 0.98 ± 0.08 ns, a value consistent with the reports in the literature.[5,32] Other TRDT measurements on InGaN epilayers[8,9] show similar slow decay behavior as in the $In_{0.05}Ga_{0.95}N$ epilayer investigated here.

B. Differential transmission of an InGaN MQW

1. Investigation of sample structure

As seen in Fig. 2, the cw PL for the MQW sample shows a single emission centered at $\sim$3.01 eV, associated with the confined QW minimum. The corresponding PLE and cw-absorption measurements indicate that the $In_{0.07}Ga_{0.93}N$ barrier energy is $\sim$3.23 eV. This barrier energy is similar to (only 30 meV below) the band edge energy measured for the $In_{0.05}Ga_{0.95}N$ epilayer, so differences in relaxation dynamics between the two samples arise from the effects of the quantum wells.

Simple 1D calculations predict the minimum confined QW energy level to be consistent with the measured 3.01 eV, given reasonable values for conduction:valence band offsets [30:70 (Ref. 33) to 75:25 (Ref. 34)] and bowing parameters [1 eV (Ref. 35)–2.6 eV (Ref. 30)]. The difference between the measured and calculated values is satisfactory given the large but uncertain PZE field strength arising from lattice mismatch-induced strain between the layers.[36]

Room temperature PLE in Fig. 2 shows clear edges at the GaN and the $In_{0.07}Ga_{0.93}N$ barrier energies consistent with cw absorption. The contribution from the confined QW states is not observed in cw absorption. However, the 83 K PLE in the Fig. 2 inset clearly shows a broad QW edge at $\sim$3.14 eV that is still weakly indicated at 3.11 eV on the 303 K PLE. Although room temperature emission is 100 meV lower than this PLE edge, a sigmoidal fit to this QW edge gives an effective band edge of 3.06 eV and a Stokes shift of only 50 meV. Shifts even larger than 300 meV have been observed for higher In composition MQWs under cw excitation.[7,12]

As in the InGaN epilayer, the strain in the barriers is decreased through Si doping.[7] MQW lateral carrier confinement arises from the formation of In-rich quantum dotlike regions in the QWs which grow with increasing In composition.[5] Such inhomogeneities have been observed for InGaN MQWs having even less than 15% In.[7,37] This carrier localization due to inhomogeneities is also expected to decrease with Si doping in the barriers.[38] As the size of In-rich regions grow, the confinement within large dots is reduced and the Stokes shift increases.

MQW SE appeared at 3.04 eV as a narrow feature on the main PL, above a threshold density of $\sim$95 μJ/cm^2 for 3.31 eV excitation. Starting from below threshold, the PL peak blueshifted as the excitation density increased. This blueshift is primarily due to increased screening of the PZE field by the increasing number of carriers and to lateral carrier confinement in the MQW. These effects combine to make the blueshift in the MQW TI PL larger than it is for the InGaN epilayer sample.

2. Spectrally integrated and resolved TRDT

To examine the relaxation of the total number of carriers, DT signals are integrated over the spectrum 2.92–3.41 eV for excitation energies 120 meV above (3.35 eV), at (3.23

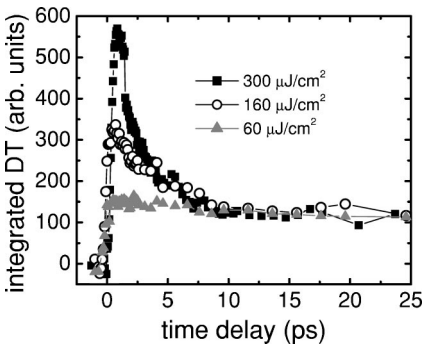

FIG. 7. Time evolution of the spectrally integrated TRDT for above (triangles), at (squares), and below barrier (circles) band gap excitations of the InGaN MQW sample at an excitation density of 300 μJ/cm^2. The integration region was 2.95 eV–3.40 eV. The inset shows the fast decay components of the data.

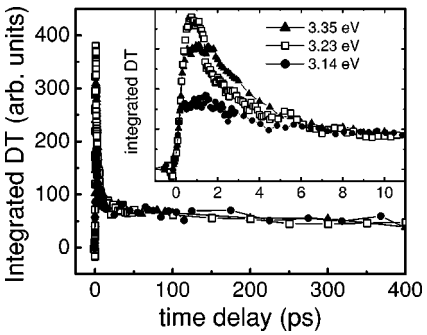

FIG. 8. Time evolution of the spectrally integrated TRDT for at-barrier excitation of the InGaN MQW sample for different pump power densities. Data were normalized to the slow decaying amplitude. With decreasing excitation density the SE-mediated fast decaying component is observed to disappear.

eV), and 90 meV below (3.14 eV) the barrier energy.[39] As seen in Fig. 7, all three spectrally integrated TRDT signals show a fast decay at early times, followed by a very slow relaxation. The fast components are observed to decay in less than 10 ps. Spectrally integrated DT data were fit by a biexponential decay function, $Ae^{-t/\tau_1}+Be^{-t/\tau 2}$, where τ_1 and τ_2 are the decay times for the fast and the slow decaying components, and A and B are the corresponding amplitudes. A fractional strength value $[f=A/(A+B)]$ is defined to observe the relative strength of the fast decaying component.

Figure 7 shows that the fractional strength (f) of the fast decaying component is largest for at-barrier excitation, and is larger for above-barrier excitation than for below-barrier excitation. As with the GaN and InGaN epilayers, the fast decay in the MQW sample is caused by the accelerated relaxation of carriers through SE. However, SE is observed even for below-barrier excitation of the MQW sample. At-barrier energy excitation data is shown in Fig. 8, where the magnitude of the fast feature is observed to decrease ($f=0.74$, 0.65, and 0.26) and its decay constant slowed (2.6, 4.6, and 13.5 ps) as the excitation density is decreased (300, 160, and 60 μJ/cm^2).[40] For a given excitation density of 300 μJ/cm^2, Fig. 7 shows that the fast feature decay times for at-, above-, and below-barrier excitations increased inversely (2.6, 2.6, and 3.7 ps, respectively), and the magnitude of the feature decreased linearly ($f=0.74$, 0.73, and 0.56), with the strength of the PLE in Fig. 2 measured at the respective excitation energies.

SE decay times faster than 10 ps have been observed for similar MQW structures at room temperature and at 2 K.[11,24] In one study, a three-level rate equation model was also developed, consisting of 2D QW, 3D barrier, and ground (recombined) states.[11] This model suggested that the fast relaxation was due to carriers decaying from the 3D states to refill the 2D states emptied by SE. The fact that higher-energy 3D states supply carriers to lower-energy states undergoing SE has been confirmed in the GaN data in Fig. 4(a) and InGaN data in Fig. 5(a). As will be discussed below, a similar process occurs in the MQWs, in which 3D states supply carriers for the saturated 2D states undergoing SE. Thus, SE reduces the total number of carriers in a similar manner for all samples studied.

To elucidate the carrier redistribution and relaxation processes, spectrally resolved TRDT data for the InGaN MQW sample for various delays at different pump energies above, at, and below the barrier energy are shown in Fig. 9. The fast decaying ac Stark and the two-photon absorption feature at the 3.41 eV GaN energy is observed at all pump excitation energies and behaves analogously to the below GaN band gap excitation for the GaN and InGaN epilayer samples discussed above. The strength of this feature decreases both with decreasing pump intensity and increasing detuning.

In further analogy with the InGaN epilayer data, a broad bleaching is observed in the InGaN MQW barrier region (3.13–3.30 eV) for all excitation energies. The peak of the carrier distribution is observed at the 3.23 eV barrier energy. For above and near band gap excitation in Fig. 9(a) and Fig. 9(b), the blue edge of this carrier distribution rises faster (300 fs and 360 fs) than the red edge (540 fs and 560 fs) in the QWs. This is reminiscent of the carrier redistribution seen in the InGaN epilayer for above band gap excitation [Fig. 5(a)].

Likewise, the blue edge of the MQW carrier distribution, centered at the 3.23 eV 3D barrier band edge, is observed to decay much faster (10 ps) than the red edge ($>$100 ps). As with the InGaN epilayer, this initial fast decay of the blue edge corresponds to the SE-related fast decay in the spectrally integrated TRDT. However, the carriers cool down to the barrier band edge more quickly ($<$1 ps) than they do for above band gap excitation of the InGaN epilayer, resulting in a very broad (170 meV) carrier distribution extending from the GaN edge down into the QWs. This difference between epilayer and MQW barrier carrier relaxation arises because capture into the QWs removes carriers from the InGaN barrier much faster than recombination removes them from the InGaN epilayer.[20]

The role of SE-mediated carrier relaxation is most clearly seen by comparing the at-barrier excitation TRDT data for above [300 μJ/cm^2, Fig. 9(b)] and below [60 μJ/cm^2, Fig. 9(d)] threshold. In the first 1 ps, the above threshold data exhibit a large, asymmetric carrier distribution, indicating the greater carrier concentration in the barriers and the role of SE

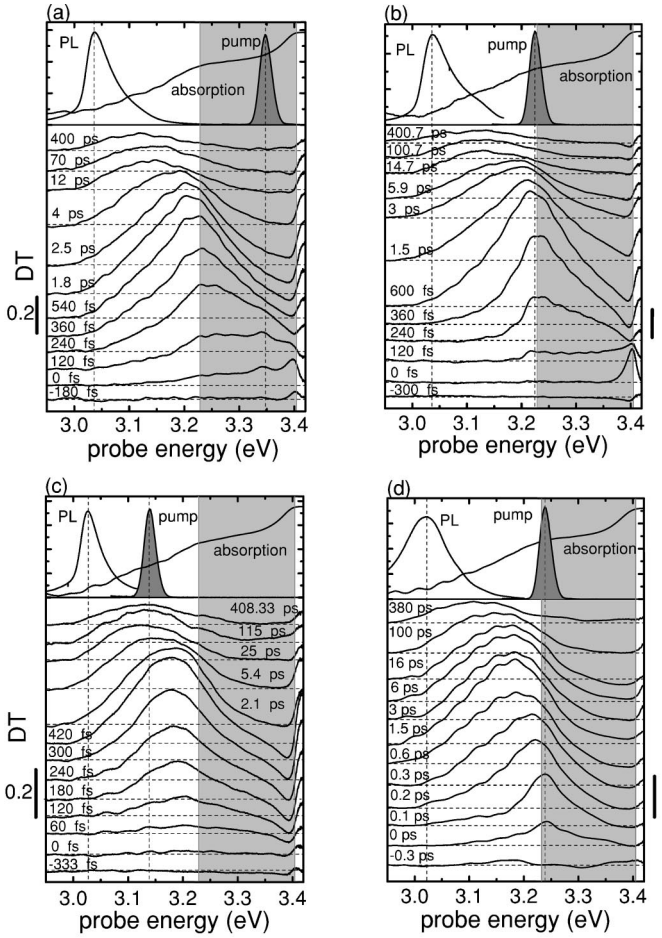

FIG. 9. Spectrally resolved TRDT for 120-meV above- (a), at- (b), and 90 meV below (c) -barrier energy excitations at various delays for an excitation energy density of 300 μJ/cm^2. Pulsed absorption shows a clear absorption edge at $\sim$3.23 eV, and the shaded regions indicate the states between the barrier and the GaN band edges. (d) TRDT data for at-barrier excitation with a lower excitation density of 60 μJ/cm^2. The vertical bars on the sides indicate a DT magnitude of 0.2.

in effectively depleting the higher-energy barrier states faster than the band edge barrier states. Although carrier capture is apparent, a large percentage of carriers remains in the barrier region while SE is operating. By contrast, the below threshold TRDT data indicates a more symmetric carrier distribution whose relaxation rates are much less sensitive to carrier energy and whose peak drops below the barrier band energy in only 300 fs. By 1.5 ps, the below threshold carrier distribution is fully 50 meV below that of the above threshold case, and the barriers are virtually depopulated. It may be surmised that SE assists in the carrier capture process by quickly depopulating QW states which are refilled by captured barrier band edge carriers which in turn are refilled by higher-energy carriers in the barriers. The normal cooling of the carrier distribution observed below threshold is altered above threshold by SE through the continued emptying of energetically accessible states near the barrier band edge. However, by 6 ps when SE is over, the distributions appear quite similar and exhibit the same relaxation behavior thereafter.

In addition to elucidating the action of SE and carrier redistribution, Fig. 9 reveals the mechanism of QW carrier capture. Due to their higher density of states, holes are expected to be captured from the 3D barriers to the 2D QW levels much faster than the electrons.[41] The 100 fs pulse widths used here limit our observations to the electron capture. After 240 fs in Fig. 9(a) and Fig. 9(b), a significant number of carriers is observed at and above the barriers for both above- and at-barrier excitations, while carriers are just beginning to appear in the QWs. As shown in Fig. 10, the carrier distribution at the 3.23 eV barrier band edge peaks in $\sim$0.5 ps, while the carrier distribution at the QWs (3.11 eV) reaches its maximum in $\sim$0.8 ps. This delay of 0.3 ps confirms that the carriers are reaching the barriers faster than the rate at which they arrive at the QWs, an indication of the electron capture process. This result is consistent with previous measurements of electron capture time (340–510 fs) using degenerate TRDT spectroscopy.[20]

In addition, degenerate TRDT showed optimal emission efficiency and the most efficient carrier capture occurred when the carrier injection was within $\pm$50 meV of the 3.23 eV barrier energy.[20] Similar to the cw-absorption data in Fig. 2, the pulsed absorption spectrum in Fig. 9 clearly shows an 100 meV-wide peak centered at 3.23 eV. This broad absorption suggests potential fluctuations in the barriers due to the compositional inhomogeneities. The spectrally integrated DT data obtained here verifies that the most efficient carrier capture occurs for pump energies near the barrier energy.

Measurements by Satake *et al.*[11] also show a broad distribution of carriers around the barrier energy and SE-related decays faster than 5 ps in the spectrally resolved DT. However, the QW capture rate could not be observed. Other studies on InGaN-based laser diode structures by Kawakami *et al.*[10,24] also observed the same fast carrier accumulation at the barriers and much slower SPE decay from the QWs. It is not clear if those samples, excited at power densities above the SE threshold, show the same initial fast decay feature in the spectrally integrated DT signals as that seen here. However, carrier capture to the lower-energy localized QW states appears to occur in less than 1 ps, similar to our measurements. Surprisingly, a sizable, narrowly distributed carrier population remains at barrier energies for at least 200 ps in their samples, which they claim is due to the capture of carriers in a high-lying, nearly delocalized QW state. This feature bears some similarity to the long-lived excitonic relaxation in GaN interfacial traps observed in our InGaN epilayer TRDT data in Fig. 5. By contrast, the distribution of carriers observed in Fig. 9 for our MQW sample is broad and quickly decaying due to rapid carrier capture from the broad barrier energy band edge.

For a below-barrier excitation energy of 3.14 eV, Fig. 9(c) shows that total carrier generation is smaller, and the peak carrier distribution appears at a slightly lower energy than that for the other two excitation energies. Indeed, the MQW carrier distribution peaks 50 meV below the barrier edge, unlike that observed for below band edge excitation in the InGaN epilayer. Nevertheless, both the InGaN and MQW

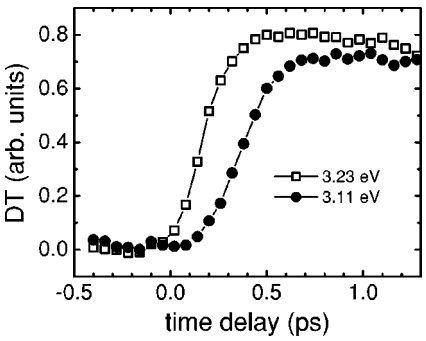

FIG. 10. Normalized DT at the barrier band edge (3.23 eV, squares) and at the QW band edge (3.11 eV, circles) for at-barrier energy excitation (300 μJ/cm^2). The rise of the latter DT is slower than the rise of the former, indicating electron capture into the confined QW states.

carrier distributions reach their maximum in a very short time ($\sim$400 fs), and the rise times for both blue and red edges of the respective carrier distributions are similar [Fig. 5(b) and Fig. 9(c)]. This behavior contrasts with the above- and at band gap excitation for the MQW in which the blue side rises faster than the red side. Furthermore, the fast decaying component of the spectrally integrated DT for the below-barrier excitation (Fig. 7) is smaller than for the other two excitations, indicating a weaker carrier decay through SE. Accordingly, the blue edge decay of the TRDT signal in Fig. 9(c) is not noticeable.

In all cases, the fast decaying component in the spectrally integrated TRDT signal disappears as the carrier density falls below the SE threshold, and emission goes from SE to SPE.[10,11,24] After SE ends (5–10 ps), the carriers at the QW band edge recombine only through SPE, and carriers at higher energies relax quickly to replace those lost at the QW band edge. For all excitations, this is observed as the redshift of the bleaching. The carrier distribution cools and redshifts to the $\sim$3.11 eV QW band edge after 400 ps. In addition to carrier recombination in the QWs, the redshift of the carrier distribution is also partly due to the reduced screening of the PZE field as carrier density decreases through SPE.[10] An exponential fit to the spectrally resolved data at 3.11 eV gives a decay constant of 0.66 ± 0.06 ns, consistent with the 0.69 ns value from previous degenerate TRDT measurements.[20] The slow decay constant from the spectrally integrated TRDT is slightly smaller (0.54 ± 0.07 ns), but agrees satisfactorily when the carrier redistribution through different channels is taken into account.

IV. CONCLUSIONS

In summary, nondegenerate TRDT spectroscopy was performed on GaN and InGaN epilayers, and an InGaN MQW. All the samples were observed to have SE features for excitation densities above a pump threshold density of $\sim$100 μJ/cm^2. Spectrally integrated TRDT data showed the effects of SE-mediated decay, which occurred in $<$10 ps for above band gap excitations. These fast decays were accompanied by carrier relaxation from higher- to lower-energy states which were emptied in turn by SE. After the total carrier density was reduced below threshold, SE disappeared and a slow relaxation through SPE was observed. For GaN, a spectrally narrow distribution of carriers decayed by SE at the band edge in 6 ps. A broader carrier distribution was observed for the InGaN sample which subsequently narrowed and decayed to the InGaN band edge through SE in $<$14 ps. Carrier recombination through spontaneous emission was observed with a time constant $<$1 ns.

Photoexcitation above, at, and below the barrier energy for the MQW sample showed more complex relaxation pathways. Spectrally integrated TRDT signals for above- and at-barrier band gap energy excitations demonstrated SE as a fast decaying component in the first 10 ps. The strength and decay times of the SE feature were seen to vary as a function of excitation energy and density. For a given excitation density, the decay times varied inversely with the PLE magnitudes for the respective excitation energy. SE was observed to depopulate the higher-energy barrier states faster than the lower-energy barrier states through a process of cascaded refilling. Once SE ended, carrier capture and spontaneous emission from carrier recombination cooled the carrier distribution into the wells and toward the lowest-energy QW state. The wavelength-nondegenerate TRDT data at QW and barrier energies provided sub-ps values for the electron capture time and $\sim$660 ps for the recombination time. These values agree well with previous degenerate TRDT measurements on the same MQW sample.[20]

ACKNOWLEDGMENT

The authors would like to thank Steven DenBaars, Stacia Keller, and Amber Abare from the University of California, Santa Barbara for supplying the samples, and Arup Neogi for helpful discussions. This work was supported by the Army Research Office.

*Email address: everitt@aro.arl.army.mil

[1] S. Nakamura and G. Fasol, *The Blue Laser Diode* (Springer, Berlin, 1997) and references therein.

[2] S. Nakamura, M. Senoh, N. Iwasa, and S. Nagahama, Jpn. J. Appl. Phys., Part 2 **34**, L797 (1995).

[3] S. Nakamura, M. Senoh, S. Nagahama, N. Iwasa, T. Yamada, T. Matsushita, H. Kiyoku, Y. Sugimoto, T. Kozaki, H. Umemoto, M. Sano, and K. Chocko, Jpn. J. Appl. Phys., Part 2 **36**, L1568 (1997).

[4] J.C. Carrano, T. Li, P.A. Grudowski, C.J. Eiting, R.D. Dupuis, and J.C. Campbell, J. Appl. Phys. **83**, 6148 (1998).

[5] S. Chichibu, T. Sota, K. Wada, and S. Nakamura, J. Vac. Sci. Technol. B **16**, 2204 (1998).

[6] E. Berkowicz, D. Gershoni, G. Bahir, E. Lakin, D. Shilo, E. Zolotoyabko, A.C. Abare, S.P. DenBaars, and L.A. Coldren, Phys. Rev. B **61**, 10 994 (2000).

[7] S.F. Chichibu, A.C. Abare, M.P. Mack, M.S. Minsky, T. Deguchi, D. Cohen, P. Kozodoy, S.B. Fleischer, S. Keller, J.S. Speck,

J.E. Bowers, E. Hu, U.K. Mishra, L.A. Coldren, S.P. DenBaars, K. Wada, T. Sota, and S. Nakamura, Mater. Sci. Eng., B **59**, 298 (1999).
[8] C.K. Choi, B.D. Little, Y.H. Kwon, J.B. Lam, J.J. Song, Y.C. Chang, S. Keller, U.K. Mishra, and S.P. DenBaars, Phys. Rev. B **63**, 195302 (2001).
[9] K. Omae, Y. Kawakami, Y. Narukawa, Y. Watanabe, T. Mukai, and S. Fujita, Phys. Status Solidi A **93**, 190 (2002).
[10] Y. Kawakami, Y. Narukawa, K. Omae, S. Fujita, and S. Nakamura, Appl. Phys. Lett. **77**, 2151 (2000).
[11] A. Satake, Y. Masumoto, T. Miyajima, T. Asatsuma, and M. Ikeda, Phys. Rev. B **60**, 16 660 (1999).
[12] R.W. Martin, P.G. Middleton, K.P. O'Donnell, and W. Van der Stricht, Appl. Phys. Lett. **74**, 263 (1999).
[13] P. Riblet, H. Hirayama, A. Kinoshita, A. Hirata, and T. Sugano, Appl. Phys. Lett. **75**, 2241 (1999).
[14] A. Satake, Y. Masumoto, T. Miyajima, T. Asatsuma, F. Nakamura, and M. Ikeda, Phys. Rev. B **57**, R2041 (1998).
[15] J.K. Shmagin, J.F. Muth, R.M. Kolbas, S. Krishnankutty, S. Keller, U.K. Mishra, and S.P. DenBaars, J. Appl. Phys. **81**, 2021 (1997).
[16] T.J. Schmidt, S. Bidnyk, Y.H. Cho, A.J. Fisher, J.J. Song, S. Keller, U.K. Mishra, and S.P. DenBaars, Appl. Phys. Lett. **73**, 3689 (1998).
[17] T.J. Schmidt, Y.H. Cho, G.H. Gainer, J.J. Song, S. Keller, U.K. Mishra, and S.P. DenBaars, Appl. Phys. Lett. **73**, 560 (1998).
[18] S. Bidnyk, T.J. Schmidt, Y.H. Cho, G.H. Gainer, J.J. Song, S. Keller, U.K. Mishra, and S.P. DenBaars, Appl. Phys. Lett. **72**, 1623 (1998).
[19] S. Keller, S.F. Chichibu, M.S. Minsky, E. Hu, U.K. Mishra, and S.P. DenBaars, J. Cryst. Growth **195**, 258 (1998).
[20] Ü. Özgür, M.J. Bergmann, H.C. Casey, Jr., H.O. Everitt, A.C. Abare, S. Keller, and S.P. DenBaars, Appl. Phys. Lett. **77**, 109 (2000).
[21] J.F. Muth, J.H. Lee, I.K. Shmagin, R.M. Kolbas, H.C. Casey, Jr., B.P. Keller, U.K. Mishra, and S.P. DenBaars, Appl. Phys. Lett. **71**, 2572 (1997).
[22] K. Omae, Y. Kawakami, S. Fujita, M. Yamada, Y. Narukawa, and T. Mukai, Phys. Rev. B **65**, 073308 (2002).
[23] C.K. Choi, Y.K. Kwon, J.S. Krasinski, G.H. Park, G. Setlur, J.J. Song, and Y.C. Chang, Phys. Rev. B **63**, 115315 (2001).
[24] Y. Kawakami, K. Omae, A. Kaneta, K. Okamoto, Y. Narukawa, T. Mukai, and S. Fujita, J. Phys.: Condens. Matter **13**, 6993 (2001).
[25] W.D. Herzog, G.E. Bunea, M.S. Ünlü, B.B. Goldberg, and R.J. Molnar, Appl. Phys. Lett. **77**, 4145 (2000).
[26] J.C. Holst, L. Eckey, A. Hoffman, I. Broser, H. Amano, and I. Akasaki, MRS Internet J. Nitride Semicond. Res. **2**, 25 (1997).
[27] S. Jursenas, N. Kurilcik, G. Kurilcik, A. Zukauskas, P. Prysyawko, M. Leszcynski, T. Suski, P. Perlin, I. Grzegory, and S. Porowski, Appl. Phys. Lett. **78**, 3776 (2001).
[28] C.K. Choi, J.B. Lam, G.H. Gainer, S.K. Shee, J.S. Krasinski, J.J. Song, and Y.-C. Chang, Phys. Rev. B **65**, 155206 (2002).
[29] This cooling is not observed in TRDT due to high absorption above the GaN band edge.
[30] C. Wetzel, T. Takeuchi, S. Yamaguchi, H. Katoh, H. Amano, and I. Akasaki, Appl. Phys. Lett. **73**, 1994 (1998).
[31] M.D. McCluskey, C.G. Van de Walle, C.P. Master, L.T. Romano, and N.M. Johnson, Appl. Phys. Lett. **72**, 2725 (1998).
[32] K.P. Korona, P. Prystawko, M. Leszczynski, P. Perlin, T. Suski, I. Grzegory, S. Porowski, and J. Kuhl, Mater. Sci. Eng., B **93**, 73 (2002).
[33] G. Martin, A. Botchkarev, A. Rockett, and H. Morkoç, Appl. Phys. Lett. **68**, 2541 (1996).
[34] J. Dalfors, J.P. Bergman, P.O. Holtz, B.E. Semelius, B. Monemar, H. Amano, and I. Akasaki, Appl. Phys. Lett. **74**, 3299 (1999).
[35] S. Nakamura and T. Mukai, Jpn. J. Appl. Phys., Part 2 **31**, L1457 (1992).
[36] T. Takeuchi, C. Wetzel, S. Yamaguchi, H. Sakai, H. Amano, I. Akasaki, Y. Kaneko, S. Nakagawa, Y. Yamaoka, and N. Yamada, Appl. Phys. Lett. **73**, 1691 (1998).
[37] S.F. Chichibu, A.C. Abare, M.S. Minsky, S. Keller, S.B. Fleischer, J.E. Bowers, E. Hu, U.K. Mishra, L.A. Coldren, S.P. DenBaars, and T. Sota, Appl. Phys. Lett. **73**, 2006 (1998).
[38] Y.-H. Cho, J.J. Song, S. Keller, M.S. Minsky, E. Hu, U.K. Mishra, and S.P. DenBaars, Appl. Phys. Lett. **73**, 1128 (1998).
[39] It should be noted that part of the DT signal at the GaN band edge is excluded from the spectral integration to avoid obfuscation by the ac Stark effect.
[40] Note that a tiny SE feature remains even below the threshold due to pump and sample inhomogeneities.
[41] N.S. Mansour, K.W. Kim, and M.A. Littlejohn, J. Appl. Phys. **77**, 2834 (1995).